J. Fluid Mech. (1991), *vol.* 231, *pp.* 229–256
Printed in Great Britain

Experiments on transitional boundary layers with wake-induced unsteadiness

By X. LIU† AND W. RODI
Institute for Hydromechanics, University of Karlsruhe, 7500 Karlsruhe, Germany

(Received 8 May 1990 and in revised form 2 January 1991)

Hot-wire measurements were carried out in boundary layers developing along a flat plate over which wakes passed periodically. The wakes were generated by cylinders moving on a squirrel cage in front of the plate leading edge. The flow situation studied is an idealization of that occurring on turbomachinery blades where unsteady wakes are generated by the preceding row of blades. The influence of wake-passing frequency on the boundary-layer development and in particular on the transition processes was examined. The hot-wire signals were processed to yield ensemble-average values and the fluctuations could be separated into periodic and stochastic turbulent components. Hot-wire traces are reported as well as time variations of periodic and ensemble-averaged turbulent fluctuations and of the boundary-layer integral parameters, yielding a detailed picture of the flow development. The Reynolds number was relatively low so that in the limiting case of a boundary layer undisturbed by wakes this remained laminar over the full length of the test plate. When wakes passed over the plate, the boundary layer was found to be turbulent quite early underneath the free-stream disturbances due to the wakes, while it remained initially laminar underneath the undisturbed free-stream regions in between. The turbulent boundary-layer stripes underneath the disturbed free stream travel downstream and grow together so that the embedded laminar regions disappear and the boundary layer becomes fully turbulent. The streamwise location where this happens moves upstream with increasing wake-passing frequency, and a clear correlation could be determined in the experiments. The results are also reported in a mean Lagrangian frame by following fluid parcels underneath the disturbed and undisturbed free stream, respectively, as they travel downstream.

1. Introduction

Unsteady boundary layers are encountered in many engineering applications, and they are often transitional, especially in turbomachines, where the unsteadiness originates from the rotor–stator interaction. In turbines and compressors, the flow approaching the rotor or stator is periodically unsteady due to the wakes generated by the preceding row of blades. These wakes pass through the cascade channels, thereby imposing a considerable influence on the boundary-layer development and in particular on the boundary-layer transition. This in turn affects the machine performance, the flow losses and especially the heat transfer to turbine blades. Hence, good understanding and predictability of the unsteady boundary-layer behaviour are important for improving the design of turbomachines. In order to further the understanding and provide data for verifying and improving prediction

† Present address: Pratt & Whitney Canada, Mississauga, Ontario, Canada.

methods, the present paper reports on a basic experimental study on the simplified situation of transitional boundary layers on a flat plate exposed to periodic wakes passing over the plate which are generated by moving cylinders.

Because of the great practical importance of unsteady boundary layers, quite a number of investigations have been carried out on this flow as summarized by Carr (1981) and Cousteix & Houdeville (1988). A few examples to quote are boundary-layer measurements with unsteadiness generated by rotating vanes at the tunnel exit (Karlsson 1985), by a deformable wall in the test section (Brembati 1975), and by mass removal control (Parikh, Reynolds & Jayaraman 1981). Further, an oscillating boundary layer was recently studied by direct numerical simulation (Spalart & Baldwin 1989). In most of these studies, the free stream oscillated everywhere at the same phase. This situation is simpler than that encountered in turbomachinery, where the axes of the wakes passing through the cascade channels are inclined to the blade walls (see figure 5 below) so that at different distances from the wall the free stream oscillates at different phases. Such situations have been studied experimentally in single-stage compressors (Walker 1974) and turbines (Hodson 1983; Addison & Hodson 1989*a*, *b*) and in linear compressor and turbine cascades using various wake-producing devices such as a rotating spoke wheel (LaGraff, Ashworth & Schultz 1988; Ashworth, LaGraff & Schultz 1989) or a moving bar chain (Dong & Cumpsty 1989*a*, *b*). In the more recent work, detailed surface hot-film and hot-wire measurements were taken which yielded, apart from informative signal traces, ensemble-average mean and stochastic fluctuations and hence important information on transition. However, the flow situation in these studies of boundary layers on blades was complicated by the influence of streamwise pressure gradients, curvature, in some cases by the occurrence of separation (Dong & Cumpsty 1989*a*, *b*) and in the real cascades possibly also by three-dimensional effects.

For a fundamental study of transition under the influence of passing wakes, experiments on two-dimensional boundary layers on a flat plate without the influence of pressure gradients are desirable. In a series of experiments, Pfeil and co-workers (Herbst 1980; Pfeil, Herbst & Schröder 1983; Schröder 1985) investigated this situation, with the periodic wakes generated by a rotating squirrel cage. They reported hot-wire signal traces and mainly time-averaged mean velocities and total fluctuations (periodic plus stochastic). Herbst (1980) did not have computer-supported signal processing and could therefore only obtain ensemble-averaged information at one station. This was helpful in understanding the flow phenomena but did not allow a complete picture to be formed. Based on their measurements, Pfeil *et al.* (1983) developed a conceptual transition model which is largely supported by the present measurements. According to this model, the wakes passing over the plate act as generators of turbulent spots or, more correctly, stripes, i.e. the stochastic turbulence in the wakes induces such stripes much earlier than the spots occurring in natural transition without free-stream disturbance due to wakes. The stripes propagate downstream, with the leading and trailing edges moving at different speeds so that the stripes merge. Before the merging, the boundary layer is intermittently turbulent and laminar and after the merging, transition is complete and the boundary layer is turbulent at all times. Pfeil *et al.* (1983) measured the leading and trailing edge propagation velocities to be respectively 0.75 and 0.54 of the free-stream velocity. The turbulent stripes were also tracked by LaGraff *et al.* (1988) and Ashworth *et al.* (1989) with the aid of heat-transfer measurements, and they found that the leading edge is convected at $0.88U_{\inf}$ and the trailing edge at $0.5U_{\inf}$, where $U_{\inf}$ is the undisturbed velocity of the approach flow. These values are

the same as measured by Schubauer & Klebanoff (1955) for turbulent spots occurring in natural transition. Dong & Cumpsty (1989*a*, *b*) tested various simple prediction models for transition and found that none of the models could describe transition well when this was initiated by moving wakes.

The research described in this paper was undertaken to provide more detailed experimental information on boundary-layer transition under the influence of passing wakes for the fundamental situation of a flat-plate boundary layer, to study the influence of the frequency of the passing wakes, and to provide data for testing existing transition models and for developing improved ones. Further, all previous investigations used an Eulerian approach to the problem, i.e. the time variation of various quantities at fixed points was characterized by the intermittent behaviour of the boundary layer in the initial region before transition is complete. This behaviour, which disappears only after the completion of transition, is conceptionally difficult to capture in a prediction model. In the present study, the high resolution of the measurement results both with respect to time and space allowed the unsteady transition phenomena to be observed in a mean Lagrangian frame. Thereby, one moves downstream with certain fluid elements of the boundary layer and observes how these undergo transition; in particular it is informative to observe the path of elements underneath the wake-disturbed free stream and underneath the undisturbed free stream. This way some of the complexities occurring in the Eulerian approach can be avoided and the transition process can be related better to the well-understood steady situation, which facilitates the description by a theoretical model.

2. Experimental set-up and measurement technique

The experiments were carried out in a low-speed wind tunnel with a test cross-section of 750×750 mm and a turbulence level below 0.3%. As shown in figure 1, a 550 mm long flat plate was mounted in the downstream part of the test section spanning the whole 750 mm width. The plate has a 4 mm leading-edge radius and was fixed at an angle of $-3°$ (nose downward) relative to the tunnel centreline in order to avoid leading-edge separation. As a consequence, the flow over the plate was slightly accelerating.

The unsteady free-stream flow with wakes passing periodically over the plate was generated by cylinders moving across the leading edge on a rotating squirrel cage, as sketched in figure 1. This device generates two-dimensional wakes but has the drawbacks that the cylinders do not move linearly across the oncoming flow and that both upward- and downward-moving cylinders generate wakes which interact. The first disadvantage is not a serious one since the thickness of the region of interest (boundary layer) is small compared with the diameter of the squirrel cage. The second problem is potentially more serious and will be addressed in some detail in §3.2. Both problems could be avoided by using a moving-bar chain device (Dong & Cumpsty 1989*a*, *b*) but this is mechanically much more complicated and difficult at high passing frequencies and could not be fitted to the existing wind-tunnel set-up.

It is known that the characteristics of wakes behind circular cylinders are in close correspondence with those behind blade profiles of equal drag. This can be confirmed by comparing the cascade-wake data of Raj & Lakshminarayana (1973) with the standard data for wakes behind circular cylinders. Hence, the wakes generated by the squirrel cage can be considered as a good simulation of the wakes stemming from a rotor cascade. It should be added that when the wakes reach the flat plate they have no shedding characteristics and are 'far wakes'.

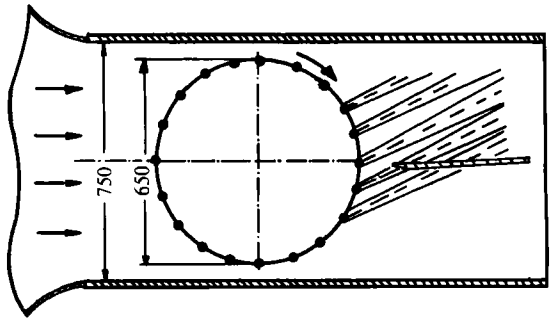

FIGURE 1. Flow configuration (dimensions in mm).

The design of the wake-generating squirrel cage device followed closely that of Pfeil *et al.* (1983) and is illustrated in figure 2. A continuously adjustable DC motor drives the long shaft (1). Through the gears and the cog belt (2) the two shafts (3) on each side of the test section (4) are synchrodriven. Each of the shafts (3) is supported by two bearings and drives the large rotating disks (5) on each side. Circular cylinders (6) spanning the test section are fixed across the two rotating disks on a 650 mm diameter circle. The two rotating disks (5) and circular cylinders (6) form the squirrel cage. Inside the cage, on each side a stationary disk (7) is mounted. The cylinders move in the gap between this stationary disk and the tunnel sidewall so that no rotating sidewall boundaries are generated. Disk (7) is supported by a stationary shaft (8) which is mounted inside the hollow shaft (3) and is supported by two bearings between (8) and (3). Shaft (8) is fixed to the supporting frame on the outer end. A rubber seal (9) prevents the air from leaving the test section. It is important to note that the whole squirrel cage assembly has no direct contact with the wind tunnel so that good operation stability is achieved.

The boundary layer developing on the flat plate surface under the influence of the passing wakes was measured in detail for altogether seven different test cases. In these, the number of cylinders mounted on the disks and the rotation speed, yielding together the passing frequency and the distance between downward-moving cylinders and the leading edge were varied. The details are given in table 1. For all test cases, the unit Reynolds number $Re = U_{\inf} \times 1/\nu$ was 9.9×10^5 and the cylinder diameter was 4 mm. The cylinders were all equally spaced. In order to check the two-dimensionality of the flow, oil flow visualization and transverse-flow surveys using a hot-wire probe were conducted and it was found that the flow velocity was uniform over the central 80% of the 750 mm plate span.

The flow velocity was measured with a DISA 55 M10 hot-wire anemometer and a DISA 55P14 single-wire probe. With the traverse gear used, the hot-wire probe could be positioned with an accuracy of 0.05 mm. The closest measurement point above the plate surface was 0.3 mm. The hot-wire signal was linearized through a DISA 55M25 linearizer and then fed for data acquisition into an HP 1000 computer through a 100 Kwords/s AD converter. The data acquisition was triggered by a one-per-revolution signal from a photocell. Each cylinder-passing period was divided into 360° in terms of the oscillation phase angle. The measured instantaneous velocity was processed on-line with the HP 1000 computer to yield the following quantities:

$$U = \langle U \rangle + u' = \bar{U} + \tilde{u} + u'. \tag{1}$$

Here, U is the instantaneous velocity, $\langle U \rangle$ is the ensemble-averaged velocity which

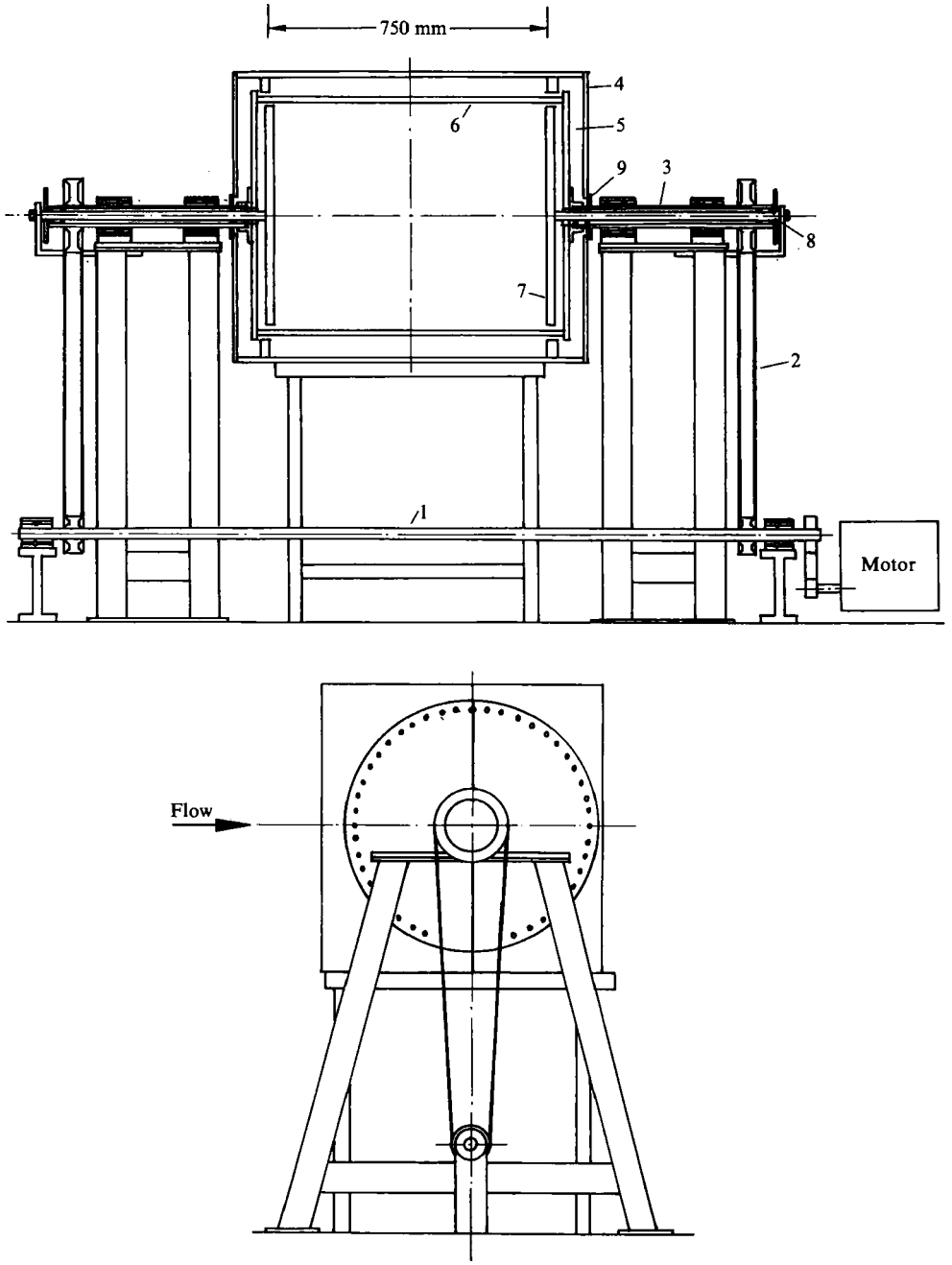

FIGURE 2. The squirrel cage: for detailed description see text.

is composed of the time-averaged value $\bar{U} = \overline{\langle U \rangle}$ and the periodic fluctuation $\tilde{u}$, and u' is the turbulent fluctuating component. The ensemble-average value is determined by sampling at constant phase from the following formula:

$$\langle U \rangle = \frac{1}{N} \sum_{i=1}^{N} U_i \quad \text{(at a fixed phase angle)}, \tag{2}$$

Case no.	1	2	3	4	5	6	7
f (Hz)	0	20	40	60	120	120	100
Number of cylinders	0	4	8	12	24	24	24
Speed of cylinders (m/s)	0	10.2	10.2	10.2	10.2	10.2	8.5
Plate position (mm)	152	152	152	152	152	100	100

TABLE 1. Test cases

where N is the number of samples. In the same way, the ensemble-averaged turbulent fluctuating velocity is obtained from

$$\langle u'^2 \rangle = \frac{1}{N} \sum_{i=1}^{N} (U - \langle U \rangle)_i^2 \quad \text{(at a fixed phase angle)}. \tag{3}$$

In order to get a converged ensemble average, the number of samples N must be large enough. In the present measurements, $N = 400$ was used for which convergence was found to be satisfactory. Typical ensemble-averaged quantities are shown in figure 14. The curves are smooth and display good periodicity. From the profiles of the ensemble-averaged velocity, the following ensemble-averaged integral parameters were determined:

$$\langle \delta^* \rangle = \int_0^{\langle \delta \rangle} (1 - \langle U \rangle / \langle U \rangle_e) \, dy, \tag{4}$$

$$\langle \theta \rangle = \int_0^{\langle \delta \rangle} \langle U \rangle / \langle U \rangle_e (1 - \langle U \rangle / \langle U \rangle_e) \, dy, \tag{5}$$

$$\langle H \rangle = \langle \delta^* \rangle / \langle \theta \rangle. \tag{6}$$

Further, the boundary-layer thickness $\langle \delta \rangle$ was evaluated as the wall distance where the ensemble-averaged velocity reached 99% of the corresponding free-stream velocity. The time-averaged values of these quantities were then determined by averaging over one period and so were time-averaged r.m.s.-values of the periodic and turbulent fluctuations.

3. Presentation and discussion of results

3.1. *Steady flow*

Measurements were carried out first for a flow situation without moving cylinders placed in front of the plate so that a steady flow resulted (test case 1). The flow near the leading edge of the slightly inclined plate behaves as sketched in the streamline picture of figure 3, which was derived from measurements of the velocity profiles at various x-stations in front of and above the plate. Very near the leading edge, a stagnation flow develops, and the flow bends from the direction parallel to the tunnel walls to the direction parallel to the plate wall. Owing to the slightly inclined plate, the channel formed by the upper surface of the plate and the tunnel walls is mildly converging, resulting in a small acceleration of the free stream, which can be seen from the development of the velocity measured at a wall distance $y = 10$ mm shown in figure 4. However, the initial acceleration is due to recovery from the stagnation flow. The free-stream turbulence level was 0.3%.

Figure 4 also displays the axial development of the displacement thickness of the boundary-layer integral parameters δ^*, momentum-thickness Reynolds number

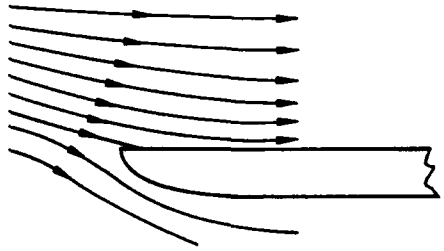

FIGURE 3. Flow around plate leading edge.

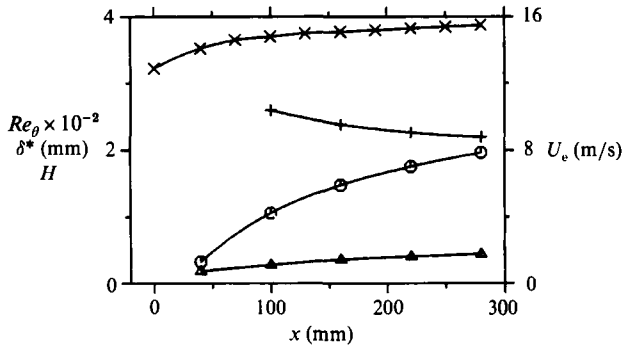

FIGURE 4. Variation of integral parameters in steady case 1: △, δ^*; ○, Re_θ; +, H; ×, U_e.

$Re_\theta = \theta U_{\inf}/\nu$ and shape factor H between $x = 40$ mm and $x = 280$ mm from the leading edge. Because the boundary layer is still rather thin at $x = 40$ mm, at this station not enough measurement points could be placed inside the boundary layer in order to determine the shape factor with any certainty. The boundary-layer thicknesses can be seen to increase with increasing x, but not quite at the rate predicted by the Blasius formula for laminar boundary layers in zero pressure gradient. This lower increase is due to the acceleration discussed above. The shape factor H is clearly above 2, indicating that the boundary layer is laminar. This observation is also supported by measurements of the fluctuating velocities very near the wall. The r.m.s. values of the u-fluctuations are always below 2% of the free-stream velocity, and the level does not increase much with x. Further, from signal traces, which in the cases with rotating cylinders clearly showed turbulent bursts when the boundary layer was turbulent, there were no significant fluctuations visible. No measurements were taken beyond $x = 280$ mm, but the measurements with four rotating cylinders indicate that without disturbance by cylinder wakes the boundary layer remains laminar until the end of the plate ($x = 550$ mm). This would also be expected from standard transition criteria (e.g. due to Abu Ghannam & Shaw 1980) according to which transition would take place in the present case when Re_θ increases beyond 900. As can be seen from extrapolating the Re_θ curve in figure 4, Re_θ is far from this value at $x = 550$ mm.

3.2. *Influence of secondary wakes generated by upward-moving cylinders*

As already mentioned, the generation of wakes with the aid of cylinders rotating on a squirrel cage has the disadvantage that wakes are generated in the course of both upward and downward motion of the cylinders and that these wakes interact with each other. Before the influence of the wakes on the boundary layer can be studied,

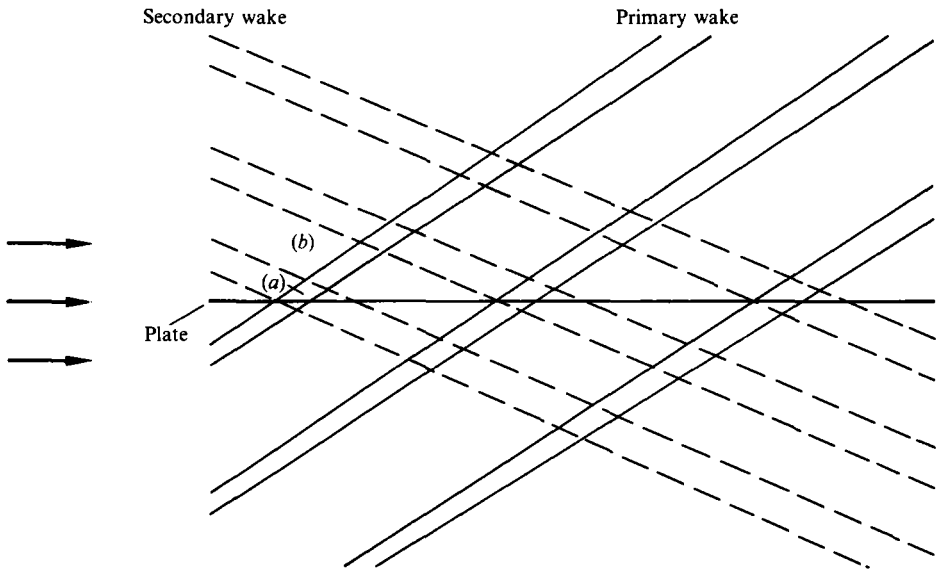

FIGURE 5. Interaction of primary and secondary wakes.

it is therefore important to know the behaviour and the influence of the secondary wakes generated further upstream by the upward-moving cylinders and the interaction with the primary wakes generated by the downward-moving cylinders. The flow pattern emerging is sketched in figure 5 showing the regions occupied by primary and secondary wakes at a certain instant, with the primary wakes inclined upward and the secondary wakes inclined downward. This flow pattern moves downstream with $U_{\inf}$, the approach velocity. As can be seen, there are regions (a) where primary and secondary wakes coincide, and at different y-distances there are regions (b) where one wake will pass after the other. This is confirmed in figure 6 by measured ensemble-averaged velocities at various wall distances y for one particular situation ($N = 8$, $x = 0$ mm). Near the wall a region (a) can be seen to exist where the wakes coincide so that only one velocity dip is present in any one cycle, whereas further away from the wall, at $y = 70$ mm and 130 mm, the two wakes pass through separately, the primary wake causing a stronger velocity dip. Further away, at $y =$ 190 mm, another coincidence region (a) exists with only one wake per cycle present. It so happens that for the cases with 4, 8 and 12 cylinders, the coincidence regions (a) extend from the wall to about $y = 40$ mm, covering the region in which detailed measurements were taken and will be reported in the following sections. Hence, the boundary layer in these cases was under the influence of one wake per cycle and there was no separate influence of the secondary, upstream wake. For the case with 24 cylinders, the upstream wakes from the individual cylinders had already merged by the time they reached the channel between the plate and the wind-tunnel wall and hence could not be discerned in velocity traces. This is therefore a clear case of only one wake per cycle passing over the plate, but with somewhat higher free-stream turbulence.

3.3. *Unsteady flow measurements in the near-wall region*

In the following, detailed hot-wire measurements are reported for the test cases 2–5 (see table 1) reaching a wall distance of 15 mm.

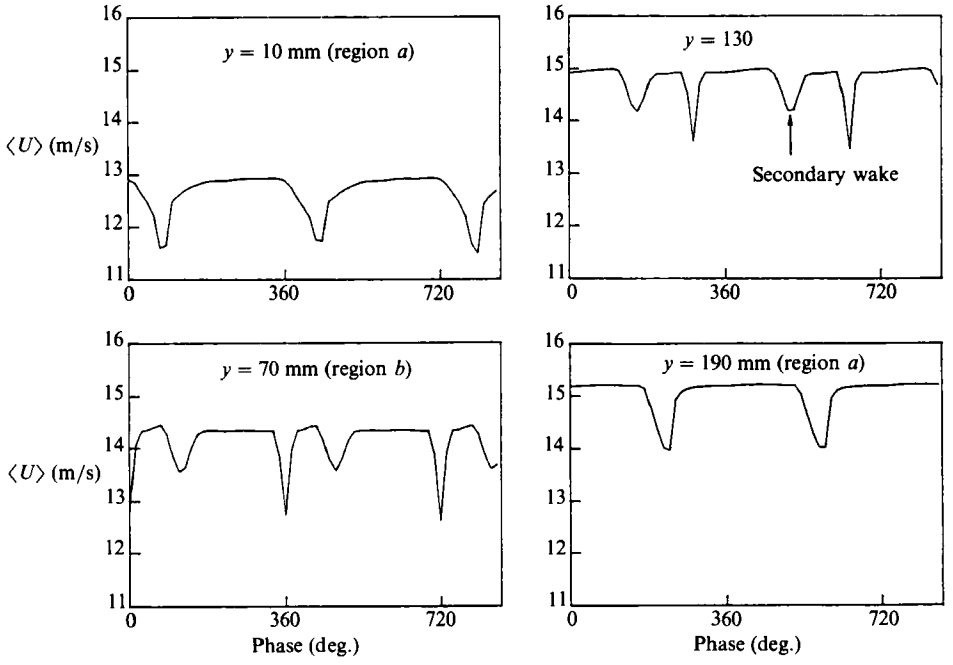

FIGURE 6. Measured time variation of $\langle U \rangle$ in regions (*a*) and (*b*) (figure 5) for case 3 at $x = 0$ mm.

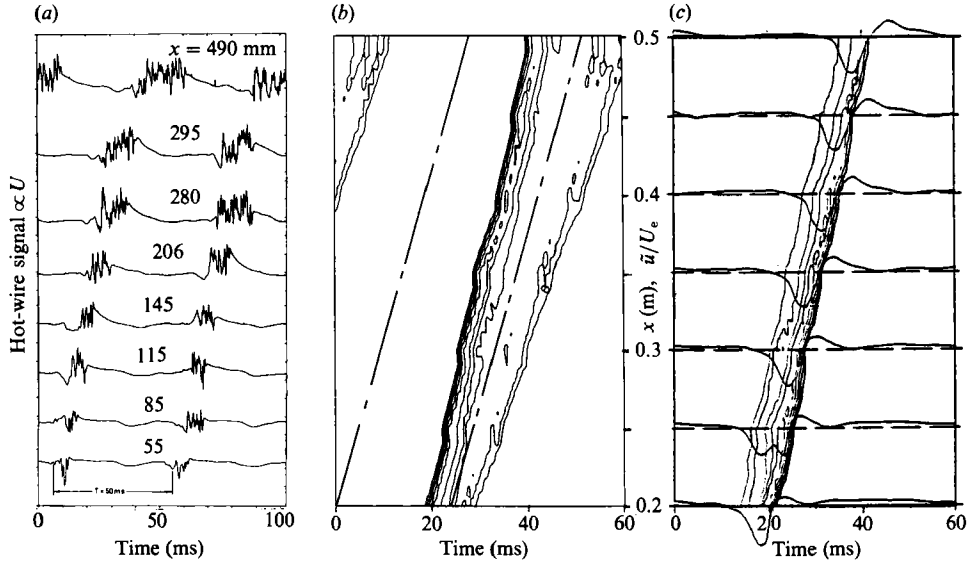

FIGURE 7. (x,t)-Diagrams for case 2 ($N = 4$): (*a*) hot-wire traces at $y = 0.3$ mm; (*b*) contours of U' at $y = 0.3$ mm; (*c*) contours of U' and variation of $\tilde{U}$ outside the boundary layer (at $y = 15$ mm).

3.3.1. (x,t)-*Diagrams*

Figures 7–10 show, respectively for $N = 4$, 8, 12 and 24 cylinders, (*a*) velocity traces and (*b*) contours of the turbulent fluctuations U' close to the wall (at the first measurement point), and in (*c*) the corresponding fluctuating velocity contours

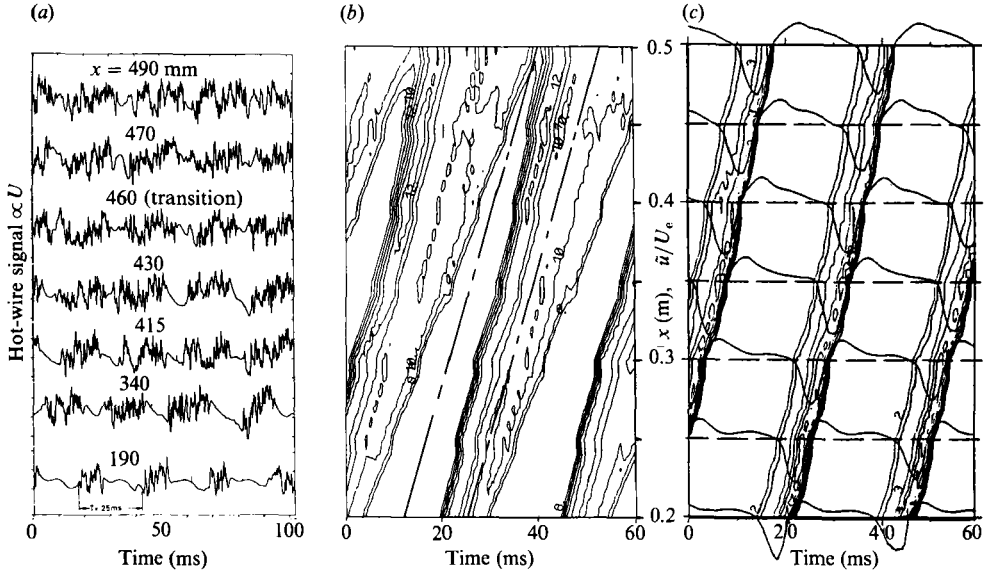

FIGURE 8. (x,t)-Diagrams for case 3 ($N = 8$): (*a*) hot-wire traces at $y = 0.3$ mm; (*b*) contours of U' at $y = 0.3$ mm; (*c*) contours of U' and variation of $\tilde{U}$ outside the boundary layer (at $y = 15$ mm).

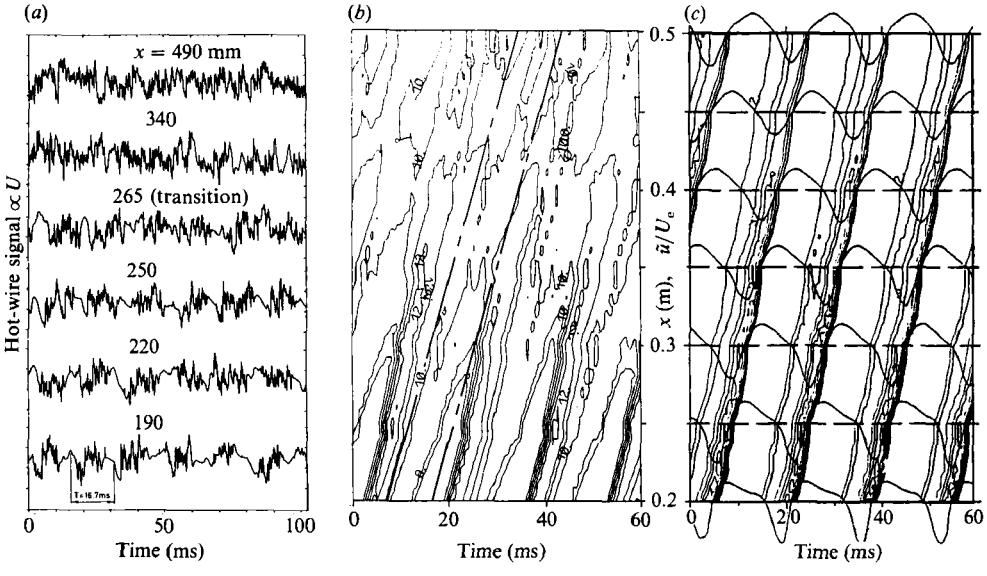

FIGURE 9. (x,t)-Diagrams for case 4 ($N = 12$): (*a*) hot-wire traces at $y = 0.3$ mm; (*b*) contours of U' at $y = 0.3$ mm; (*c*) contours of U' and variation of $\tilde{U}$ outside the boundary layer (at $y = 15$ mm).

outside the boundary layer (at $y = 15$ mm) with the variation of the periodic velocity $\tilde{U}$ at various x-distances superimposed. Here and in later figures, the symbols U' and $\tilde{U}$ stand for

$$U' = \langle u'^2 \rangle / U_{\inf}, \quad \tilde{U} = \tilde{u}/U_{\inf},$$

where $U_{\inf}$ is the undisturbed velocity of the approach flow. The results close to the

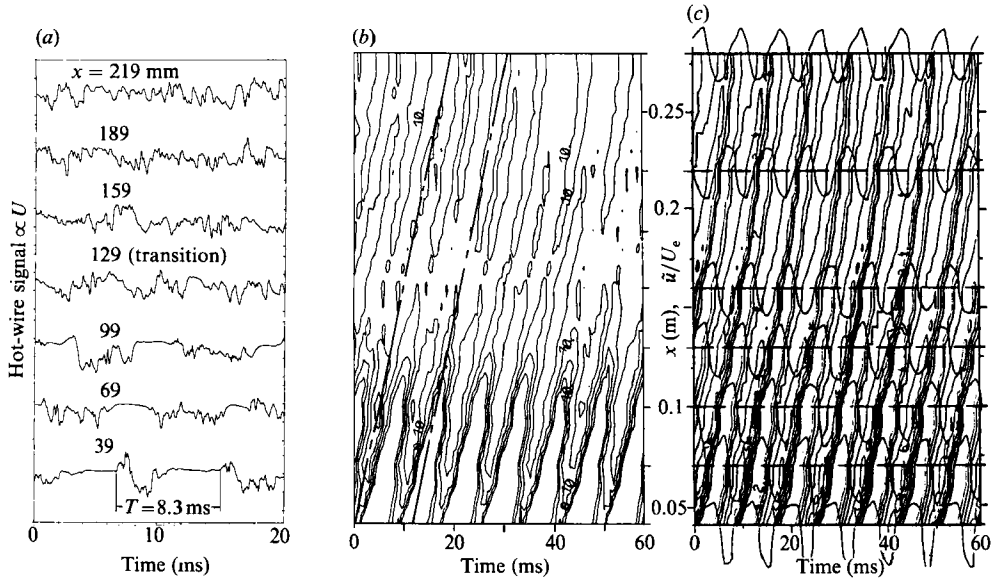

FIGURE 10. (x,t)-Diagrams for case 5 ($N = 24$): (*a*) hot-wire traces at $y = 0.3$ mm; (*b*) contours of U' at $y = 0.3$ mm; (*c*) contours of U' and variation of $\tilde{U}$ outside the boundary layer (at $y = 15$ mm).

wall give an indication of the state of the boundary layer and in particular of the turbulent patches present there, while the results for $y = 15$ mm show the wakes passing over the plate and give a picture of the free-stream conditions outside the boundary layer. Unfortunately, the traces are not available at the same timescale as the rest of the figures, and for $N = 12$ the timescale is particularly unfortunate as the wakes are too close together to be clearly discernible, but this could not be changed as the trace information was not stored. However, the unprocessed information provided by the traces is still very informative.

The behaviour of the free-stream velocity and turbulence as displayed in figure parts (*c*) is discussed first. For $N = 4$ (figure 7), clearly isolated wakes exist with undisturbed flow between them. The wake behaviour is not symmetric, with an excess velocity appearing at the trailing edge and the highest fluctuations appearing near this edge due to the largest velocity gradients there. As this behaviour is absent further away from the wall and also near the plate leading edge where the boundary layer is very thin (see figure 6) it is believed to be due to an interaction between the wake and the boundary layer. Another noteworthy feature is the virtual absence of any spreading and decay of the wakes which may again be associated with the interaction with the boundary layer, but may also be due to the observed wake being the outcome of a coincidence of primary and secondary wakes. In any case, the wake does not have the spreading and decay behaviour of single wakes in unconfined surroundings as measured by Pfeil & Schröder (1981). A similar absence of wake spreading was also observed by Addison & Hodson (1989*a*, *b*) in their single-stage turbine measurements. The wakes travel downstream at the free-stream velocity U_e which determines the inclination angle in the (x,t)-diagram ($\mathrm{d}x/\mathrm{d}t = U_e$).

When the number of rotating cylinders, N, is increased, the wakes pass of course more often, their separation in time is reduced, and the individual wakes start to interact. The undisturbed periods disappear and the periodic or ensemble-averaged

velocities are never really constant, as was the case for $N = 4$ when the wakes were still sufficiently separated. There is, however, still a fairly clear region of velocity deficit with relatively strong gradients where the turbulent fluctuations are also clearly higher than the background level. Up to $N = 12$, there is not too much difference between the individual wakes, i.e. they have about the same width and show little spreading or decay except perhaps for the fluctuation level which shows some decay. For $N = 24$, the wakes follow so closely that there are only short periods of fairly undisturbed flow between the wakes even at the first measurement station ($x = 40$ mm). In this case, there is wake spreading and decay, and by $x = 280$ mm the undisturbed regions with small gradient have virtually disappeared. This different behaviour may be due firstly to the interaction of the individual wakes but also due to the fact that in this case individual secondary wakes are no longer present but increase the background turbulence level, which in turn promotes the spreading of the primary wakes. It should be noted that, because the measurement region for the case $N = 24$ is upstream of other cases, the cut-off level in the fluctuating velocity contours in figure 10(*c*) is higher than that for the other cases (figures 7–9*c*), as otherwise no individual wakes could have been discerned. For this reason, the wakes appear thinner; had the same cut-off level been taken as in figures 7–9(*c*), then about the same wake width could have been interpreted at the same x-location, but the boundaries of the individual wakes would have overlapped.

Turning now to the near-wall behaviour, the traces and U'-contours shown respectively in figure parts (*a*) and (*b*) show that in all cases there are initially times of laminar undisturbed flow interrupted by times with considerable turbulent fluctuations. These times with turbulent fluctuations can clearly be associated with the wakes passing over the plate. The periods with turbulent fluctuations, which may be associated with turbulent stripes, increase in the downstream direction, i.e. the stripe width grows. This is the well-known phenomenon of different propagation velocities of leading and trailing edges of turbulent spots and stripes in a boundary layer, discussed for example in Pfeil *et al.* (1983). However, in the case of $N = 4$ (figure 7), the turbulent periods do not grow together until the last measurement station so that there is no complete transition in this case and laminar periods exist even at the most downstream station. The U-traces show a rather interesting behaviour in this case. At small x-positions, the instantaneous velocity U decreases when a wake passes, while it increases at larger x-positions, in each case compared with the velocity prevailing during the undisturbed periods. This different behaviour is a first indication of the fact that underneath the passing wakes the boundary layer is turbulent, extending further into the free stream but having steeper velocity gradients near the wall than the laminar boundary layer existing during undisturbed periods between the passing wakes. This is manifested by the typical ensemble-averaged velocity profiles shown in figure 11 for two times, one when the boundary layer is turbulent and the other when it is laminar. Near the leading edge, the boundary layer is rather thin and hence the first measurement point ($y = 0.3$ mm) lies in an outside region of the boundary layer where the velocity during the turbulent state is lower than during the laminar state according to figure 11. This explains why the instantaneous velocity clearly decreases at $x = 55$ mm when the wakes pass through. However, further downstream where the boundary-layer thickness is increased, the first measurement point is in a region where the velocity in the turbulent boundary layer is higher than in the laminar one because of the steeper gradients in the former near the wall so that the instantaneous velocity increases when the wakes pass through.

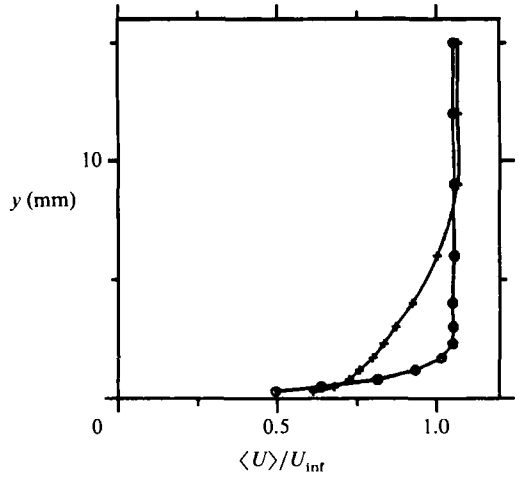

FIGURE 11. Profiles of $\langle U \rangle$ for case 2 ($N = 4$), $x = 350$ mm, in the boundary layer underneath undisturbed (○, phase = 90°, $t/T = 0.25$) and disturbed (+, phase = 245°, $t/T = 0.68$) free stream.

Starting with $N = 8$, the turbulent regions (or stripes) grow together so that the laminar regions disappear at some downstream location and the flow becomes permanently turbulent; transition can then be said to be complete. This is evident both from the traces in figure parts (*a*) and from the U'-contours in parts (*b*), and hence in fact the contour plots showing the leading and the trailing edges of the turbulent stripes in an (x, t)-diagram are similar to the graphs of Pfeil *et al.* (1983) introducing their conceptual transition model, except that they have fixed t as ordinate and x as abscissa and that in the present case the origins of the stripes are outside the graph as transition from laminar to turbulent boundary layer underneath the wakes always occurs before the first measurement station. The position where transition is complete, roughly defined by the x-location where undisturbed laminar flow regions disappear, can be determined from both the traces and from the U'-contours, and the values for each N are given in table 2 below. The transition locations determined from the contours are of course dependent on the cut-off level. For $N = 8$ and 12, the measurements start at relatively large x, where the boundary layer is already fairly thick so that the first measurement point ($y = 0.3$ mm) is always in the inner region of the boundary layer and the instantaneous velocity always increases when a wake passes. This is different from the case of $N = 24$, where the measurements were taken closer to the leading edge because transition occurred much earlier.

Comparing the U'-contours near the wall (figure parts *b*) and outside the boundary layer (parts *c*), it can be seen that the wake turbulence in the free stream propagates downstream faster than the turbulent stripes near the wall. As was mentioned before, the wakes travel with the free-stream velocity while the turbulent stripes travel at a lower velocity for which values between 0.5 and 0.88 times the free-stream velocity can be found in the literature as was discussed in the Introduction. From figures 7–10 (*b*), convection velocities for the centre of the turbulent stripes have been determined to be $0.7U_{\text{inf}}$, which is about the average of the leading- and trailing-edge velocities cited in the literature. The different propagation velocities lead to a time shift in the contours which is strengthened by the fact that, according to figure 6, the wakes pass earlier at larger y-distances than at the wall.

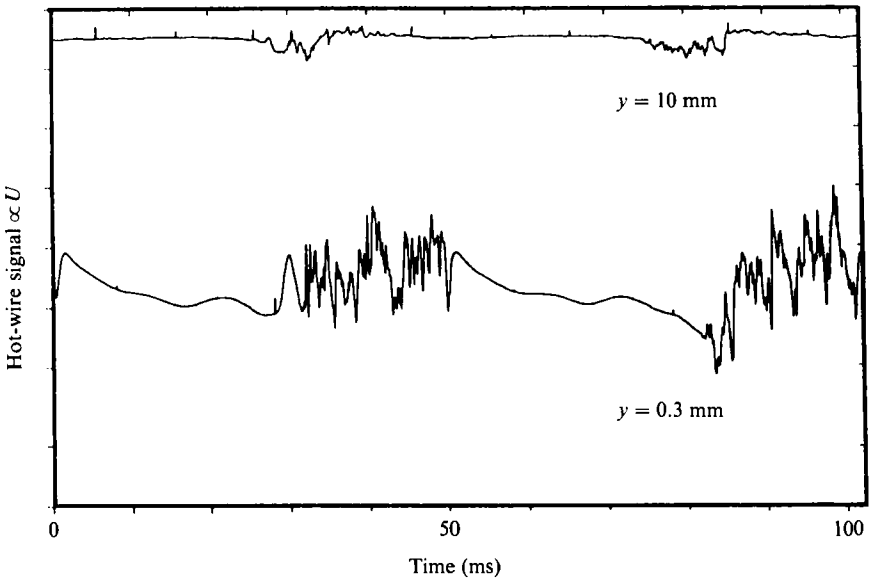

FIGURE 12. Hot-wire traces for case 2 ($N = 4$) at $x = 400$ mm.

Figure 12 compares the velocity traces for two different y-locations, one very near the wall and one outside the boundary layer for $N = 4$ and $x = 400$ mm. This figure shows clearly the decrease of the instantaneous velocity in the wake outside the boundary layer and the increase very near the wall. Further, the turbulent fluctuations can be seen to have a much higher level near the wall than in the outside wake, indicating clearly that the near-wall turbulence is not just imparted wake turbulence but is near-wall turbulence of the turbulent boundary layer. Lastly, this figure also shows the time shift in the disturbance near the wall and in the outside flow.

3.3.2. *Temporal variation of $\tilde{U}$, U' and boundary-layer integral parameters*

Figures 13–16 show respectively for the cases with $N = 4$, 8, 12 and 24 at three x-positions the temporal variation of the periodic velocity $\tilde{U}$ and the turbulent velocity U' at four wall distances as well as of the integral parameters $\langle \delta^* \rangle$, $\langle \theta \rangle$ and $\langle H \rangle$ (readers interested in larger-scale figures can obtain these from the second author). For each case, the time-averaged boundary-layer thickness $\bar{\delta}$ is also given. Outside the boundary layer (at the largest distance from the wall), the behaviour of $\tilde{U}$ and U' is as discussed already in the context of figures 7–10, except that the distribution of the turbulent fluctuations is now easier to see. There is a clear correlation between these fluctuations and the deficit in the ensemble-averaged velocity, and the peak can be seen to occur at the time of steepest velocity gradient. Considering first the case with $N = 4$ (figure 13), one can see that two velocity dips develop as one moves closer to the wall. There is some possibility that these two dips are associated with the primary and secondary wakes passing over the plate, i.e. that the coincidence of the two wakes closer to the wall is not as complete as further away. However, there is another possible mechanism which would explain the two dips. It can be seen that the trailing dip gets much stronger as one moves from the free stream into the boundary layer, and this dip is clearly associated with the change from laminar to turbulent boundary-layer velocity profiles as discussed before and as illustrated in

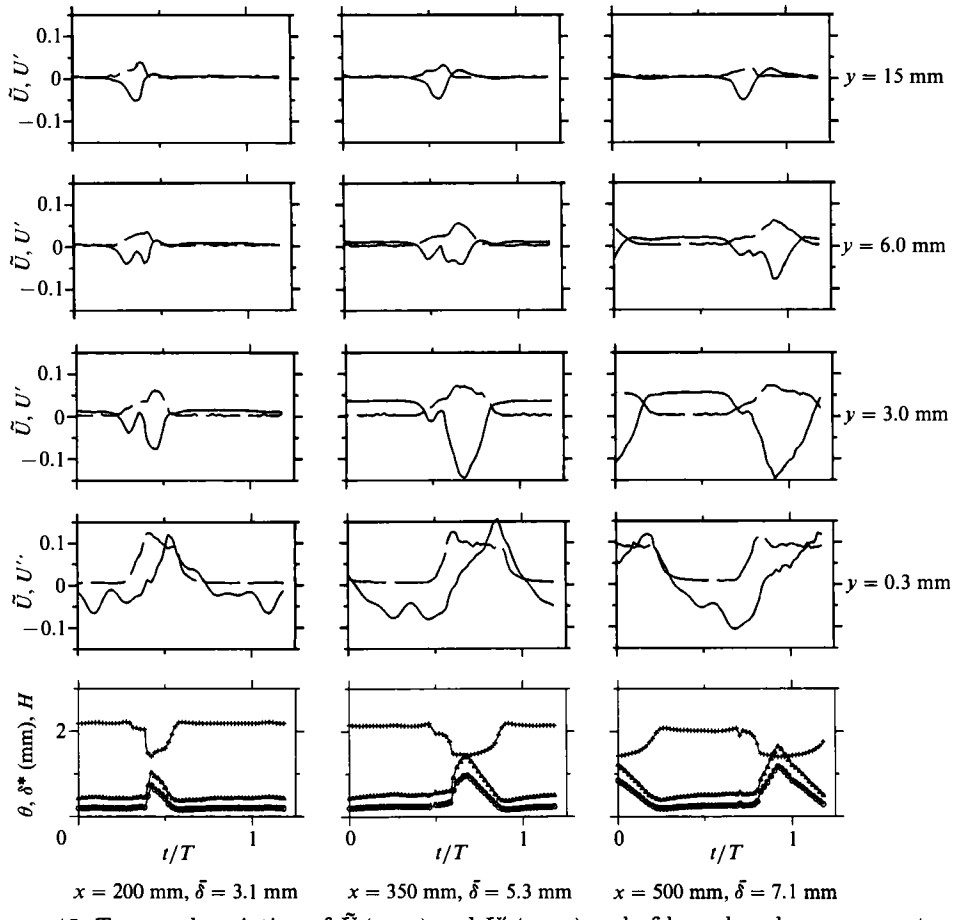

FIGURE 13. Temporal variation of $\tilde{U}$ (——) and U' (— — —) and of boundary-layer parameters $\langle\delta^*\rangle$, $\langle\theta\rangle$ and $\langle H\rangle$, △, ○ and + respectively, for case 2 ($N = 4$).

figure 11. Very close to the wall, the deficit velocity changes into an excess velocity of nearly equal size which again follows from figure 11, showing that the velocity very near the wall is higher during the times the boundary layer is turbulent than during the times when it is laminar. As the wall is approached, there is a time shift in the occurrence of velocity deficit and excess to later times, and this is due to the convection velocity in the boundary layer being lower than the free-stream velocity. A further time shift is apparently introduced by a certain time lag between the occurrence of fairly large turbulent fluctuations in the boundary layer and the development of a turbulent boundary-layer profile. This can be seen clearly from the $\tilde{U}$ and U' variations at the smallest wall distance ($y = 0.3$ mm). All this explains fairly well the behaviour of the trailing velocity dip which switches to an excess velocity very near the wall. The first, leading velocity dip may then simply be the one imposed by the free stream, of course altered by interaction with the wall and with the other dip caused by the deficit in the outer part of the turbulent boundary layer. The time shift between the two dips is due to the lower convection velocity of the turbulence causing the trailing dip in the boundary layer. The temporal variation of $\tilde{U}$ with valleys and peaks as discussed above becomes stronger as one moves downstream. This is associated with the growth of the boundary layer, and in

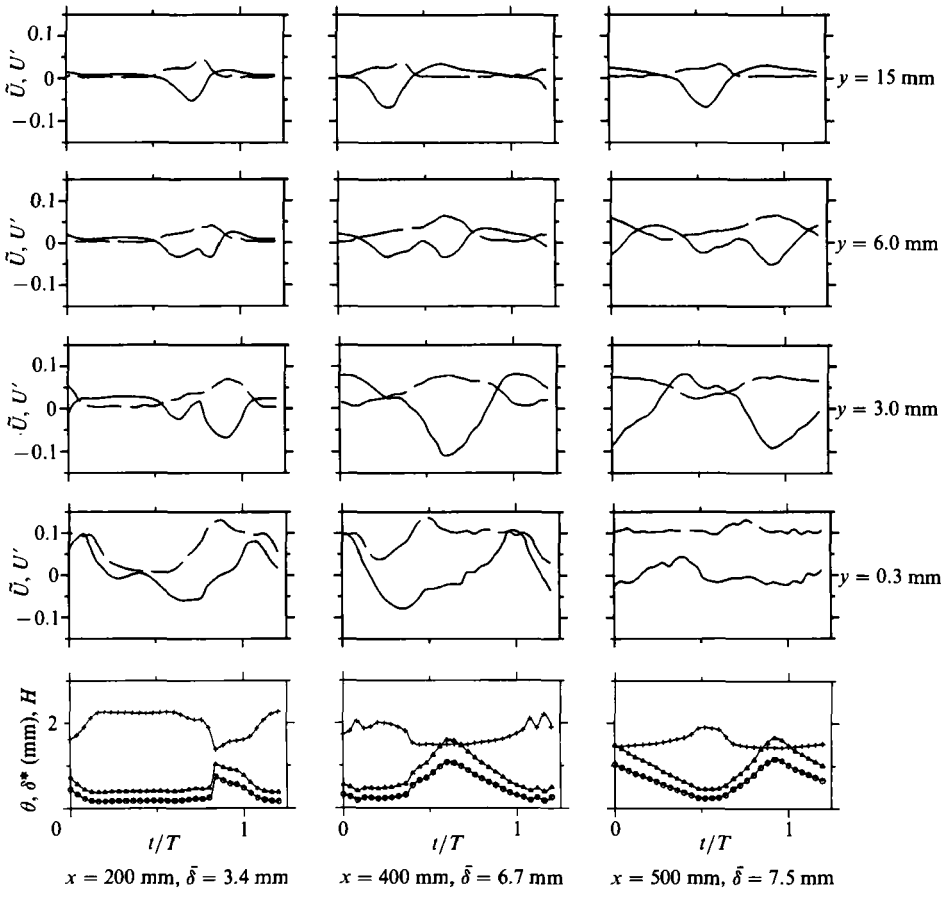

FIGURE 14. Temporal variation of $\tilde{U}$ (——) and U' (— — —) and of boundary-layer parameters $\langle\delta^*\rangle$, $\langle\theta\rangle$ and $\langle H\rangle$, △, ○ and + respectively, for case 3 ($N = 8$).

particular with the turbulent portions of it, so that the differences between the velocity profiles during laminar and turbulent periods become stronger and hence also the periodic fluctuations thereby induced. Further, the periods during which the boundary layer is turbulent can be seen to become larger with increasing downstream position.

The behaviour of the integral parameters is consistent with the picture portrayed above. During times when the boundary layer is laminar, the thicknesses $\langle\delta^*\rangle$ and $\langle\theta\rangle$ are small and the shape factor is above 2. During times when the boundary layer is turbulent, the thicknesses increase considerably and the shape factor drops to values of around 1.5, typical for turbulent boundary layers. The periods with increased boundary-layer thicknesses and lower shape factor correspond roughly with the periods of high turbulence intensity in the boundary layer and with the periods of large velocity deficit in the outer part of the boundary layer. The velocity excess very near the wall experiences some time lag with respect to these periods.

For the case with $N = 8$ (figure 14), the behaviour is rather similar but the wakes now occupy a longer portion of one cycle, and so do the turbulent stripes in the boundary layer. At $x = 400$ mm, the turbulent stripes have almost grown together as the periods with lower turbulence intensity are now rather short. The behaviour of the ensemble-average velocity is again lagging this behaviour as it still shows fairly

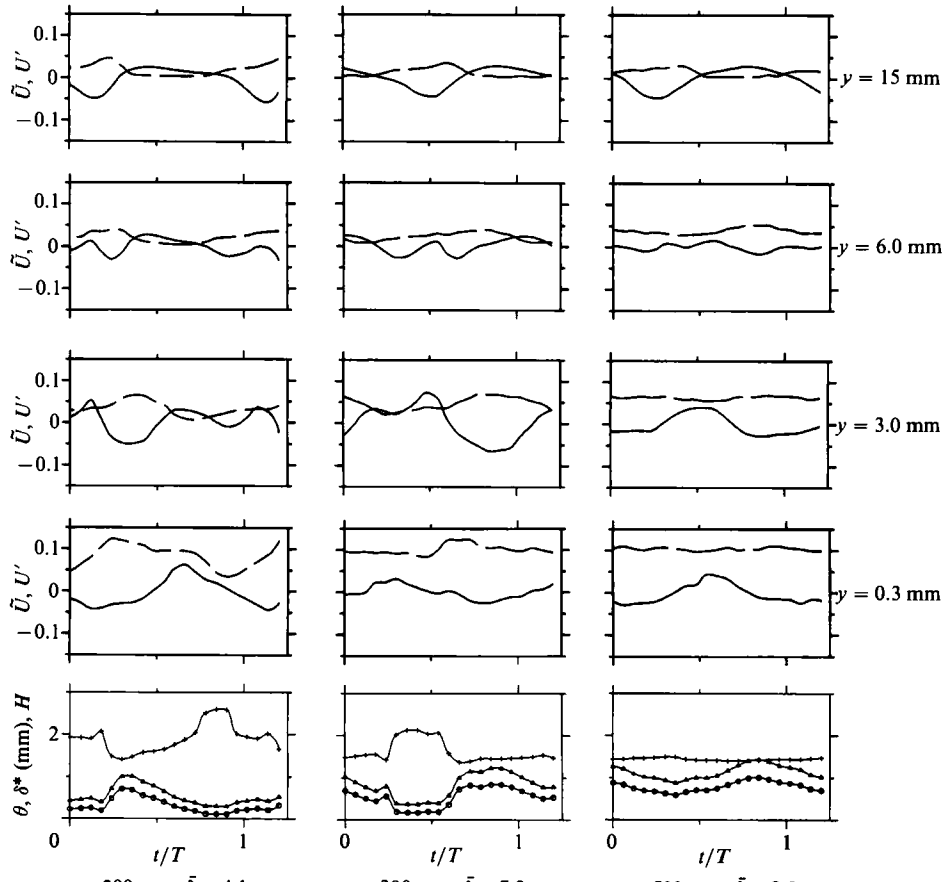

FIGURE 15. Temporal variation of $\tilde{U}$ (——) and U' (– – –) and of boundary-layer parameters $\langle\delta^*\rangle$, $\langle\theta\rangle$ and $\langle H\rangle$, △, ○ and + respectively, for case 4 ($N = 12$).

strong variations over one cycle. At $x = 500$, where the turbulent stripes are fully merged and the turbulence intensities are fairly constant over one cycle, the situation has already changed. There is now only a weak variation of the velocity very near the wall over the cycle. However, as the lower picture with integral parameters indicates, there is still considerable variation in boundary-layer thicknesses and shape factor indicating that transition is not fully complete. Correspondingly, in the outer part of the boundary layer, a considerable velocity dip still exists at times when the boundary layer is fully turbulent and hence thicker.

For $N = 12$ (figure 15), the situation is again similar, but now the turbulent stripes merge earlier and in fact by $x = 200$ mm the turbulent fluctuations near the wall have a fairly high level over most of the cycle. Here the lagging of the velocity variation behind the turbulent fluctuations very near the wall is clearly visible as the peak of the near-wall velocity in the turbulent boundary layer appears near the trailing edge of the turbulent stripe, while at the leading edge the velocity is actually below its average value. On the other hand, the velocity dip in the outer part of the boundary layer is more or less in phase with the period of high turbulent intensity and so are the boundary-layer integral parameters. At $x = 300$ mm, the turbulent stripes have already merged and U' is nearly constant at a level of 0.1, which is a typical near-wall value for turbulent boundary layers. The velocity also shows little

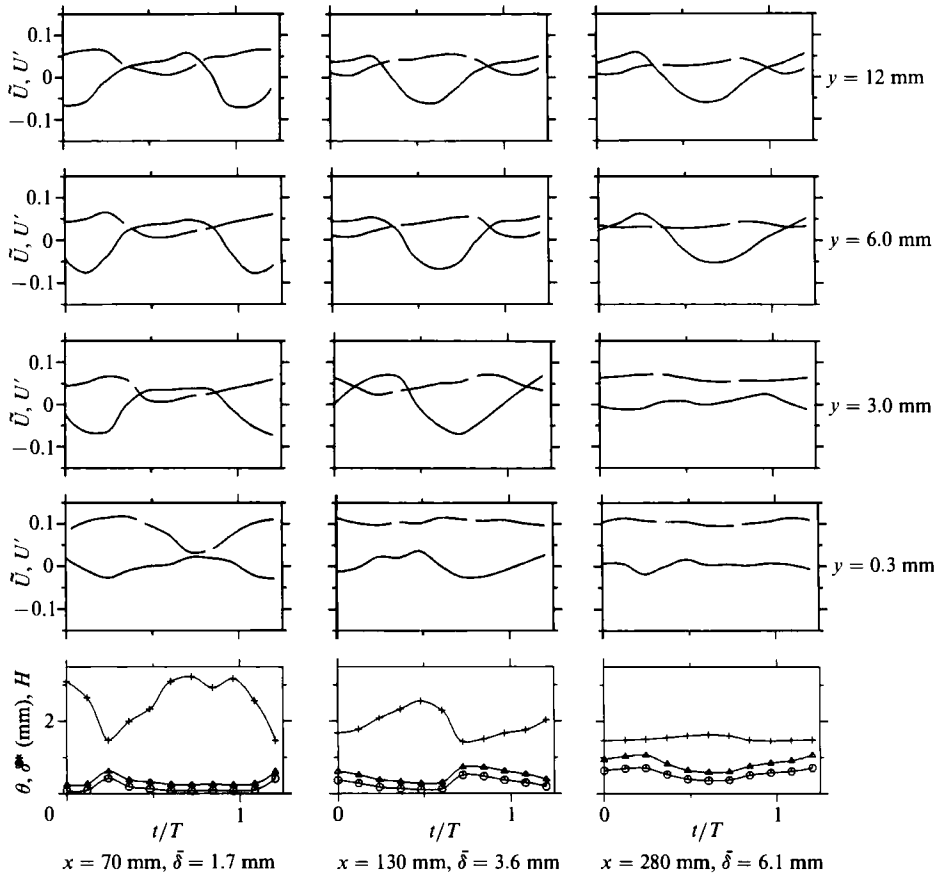

FIGURE 16. Temporal variation of $\tilde{U}$ (——) and U' (——) and of boundary-layer parameters $\langle\delta^*\rangle$, $\langle\theta\rangle$ and $\langle H\rangle$, △, ○ and + respectively, for case 5 ($N = 24$).

variation with time at the point very near the wall. On the other hand, the integral parameters again still vary considerably. Associated with this is a still fairly strong variation of the velocity in the outer part of the boundary layer. As discussed before, this indicates that transition is not complete and that the velocity distribution is still adjusting. Further downstream at $x = 500$ mm, the variations have already become considerably smaller so that now a fully turbulent state has almost been reached. Some variations of the velocity prevail, but these are now in phase with the velocity variation in the free stream, indicating that this variation is associated directly with the wake passing through this region.

For $N = 24$ (figure 16) the wake occupies more than half of one cycle and it is noteworthy that the behaviour of $\tilde{U}$ and U' in the regions outside the boundary layer does not change noticeably as the wall is approached. At the station $x = 70$ mm, the turbulent stripes have not fully merged and there is still a short period of low turbulence intensity and a somewhat longer period where the integral parameters are typical of a laminar boundary layer. However, the velocity at the point nearest to the wall shows only relatively small variation with time, and this is in phase with the variation of the velocity outside the boundary layer. This may be connected with the relatively small increase in boundary-layer thickness under the wake in this case (see $\langle\delta^*\rangle$ variations at $x = 70$ mm) but it may also be the case that the measurement

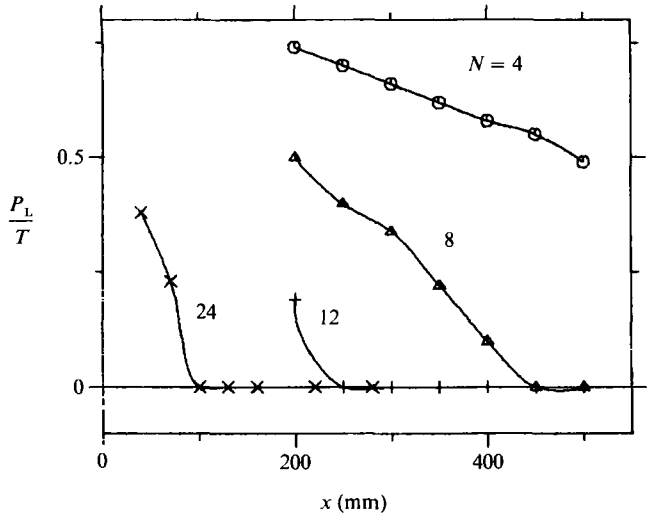

FIGURE 17. Laminar period P_L normalized by cylinder-passing period T measured at $y = 0.3$ mm.

point is near the switch-over between deficit and excess velocity described above in connection with the velocity profiles in figure 11. At $x = 130$ mm, the turbulent stripes have already merged and the turbulence intensity is fairly constant at the usual level of 0.1. The integral parameters still show a fairly considerable variation, indicating again that transition is not complete. Associated with this is the variation of the velocity in the outer part of the boundary layer. Further downstream at $x = 280$ mm, however, the variations of velocity and turbulence intensity are fairly small everywhere inside the boundary layer and so are the variations of the integral parameters, indicating that transition is complete.

In order to examine quantitatively where the turbulent stripes have merged in the various cases and where transition is complete as far as the near-wall fluctuations are concerned, the duration of the laminar periods at the measurement position closest to the wall is plotted versus x for the various cases in figure 17. The laminar period P_L is defined as the time where the relative turbulence intensity falls below a preset value, here taken as 5%. Of course, P_L depends on the value chosen for this. Figure 17 shows how the laminar periods become shorter with increasing x, indicating the growing together of the turbulent stripes, and where they become zero for the cases with 8, 12 and 24 cylinders. These values are given as transition locations in table 2 below. Another indicator of transition is the minimum value of U' during each cycle. When this increases considerably, transition in the laminar flow patches underneath the undisturbed flow occurs. Figure 18 displays the variation of this minimum of U' with x for the various cases. The location where the relative intensity has reached 90% of its value of 0.1 in turbulent boundary layers at this wall distance is also given as transition location in table 2.

3.3.3. *Mean Lagrangian treatment of boundary-layer development*

Another way of looking at the boundary-layer development is to follow individual fluid parcels in the boundary layer on their path downstream and distinguish between parcels associated with disturbed (wake) and undisturbed free stream. Boundary-layer elements travelling underneath wakes will become turbulent fairly

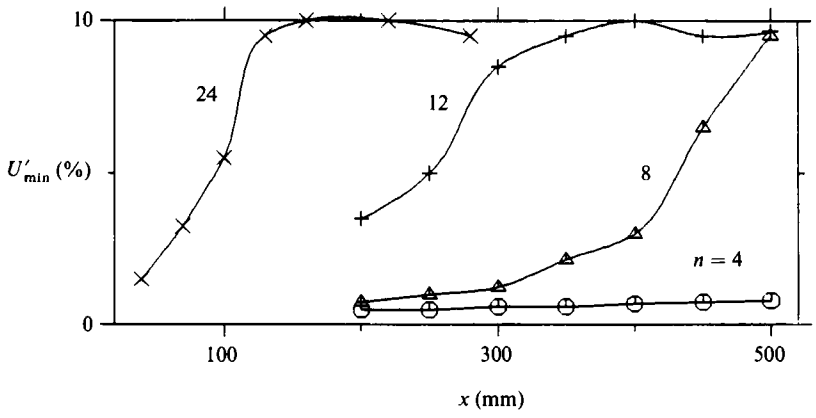

FIGURE 18. Minimum value of U' during one cycle measured at $y = 0.3$ mm.

early owing to the disturbances caused by the wake, and the turbulent stripes generated thereby will then travel downstream and grow in width as discussed above. Boundary-layer elements travelling underneath the undisturbed free-stream flow will remain laminar for much longer and, in the present experiment, will only turn turbulent where the turbulent stripes generated by the wake disturbances merge. The development of fluid parcels underneath the undisturbed and disturbed free stream can be followed in a mean Lagrangian way by plotting the measurement results along the straight dashed lines given in the (x,t)-diagrams of figures 7–10(b) which are the centrelines of the disturbed and undisturbed periods, respectively. In effect, the results plotted at a certain x-position are taken at a time

$$t = t_0 + (x - x_0)/U_c,$$

where t_0 is the time corresponding to the centre of the laminar or turbulent stripes at location x_0 (basis of inclined lines in figures 7–10b) and U_c is the convection velocity of the turbulent stripes determined from the inclination of the lines in figures 7–10(b) ($U_c = \mathrm{d}x/\mathrm{d}t$). For cases with $N = 4$, 8 and 12, $U_c = 0.7U_{inf}$ while for the case with $N = 24$ it was found that $U_c = 0.77U_{inf}$ from figure 10(b). Figure 19 shows both the development of the turbulent fluctuations at the point nearest the wall and of the shape factor as one travels with the fluid stripes underneath disturbed and undisturbed free-stream flow (along the two inclined lines in figures 7–10b). It can be seen clearly that in the stripes disturbed by the wake (triangles) the boundary layer is turbulent over the full measurement region with fairly constant values of relative turbulence intensity of 0.1 which are typical for near-wall fluctuations in turbulent boundary layers. The shape parameter is also nearly constant at a value of $H \approx 1.5$ which is also typical of turbulent boundary layers. Transition to turbulence of these stripes must have occurred upstream of the first measurement point, except in the case with $N = 24$ where both the shape factor and the hot-wire traces ($x = 70$ mm) indicate that transition is complete only at the second measurement point. Early transition underneath the passing wakes is likely to occur owing to the stochastic disturbances and not to a destabilizing pressure gradient imposed on the boundary layer by the wakes. The free-stream velocity provided in figure 4 and the mean-pressure coefficient $\bar{c}_p$ given in Liu & Rodi (1989) for case 6 clearly indicate a favourable mean pressure gradient. Measurements of the periodic pressure fluctuations ($\tilde{c}_p$) have shown that these are so small compared with the mean pressure

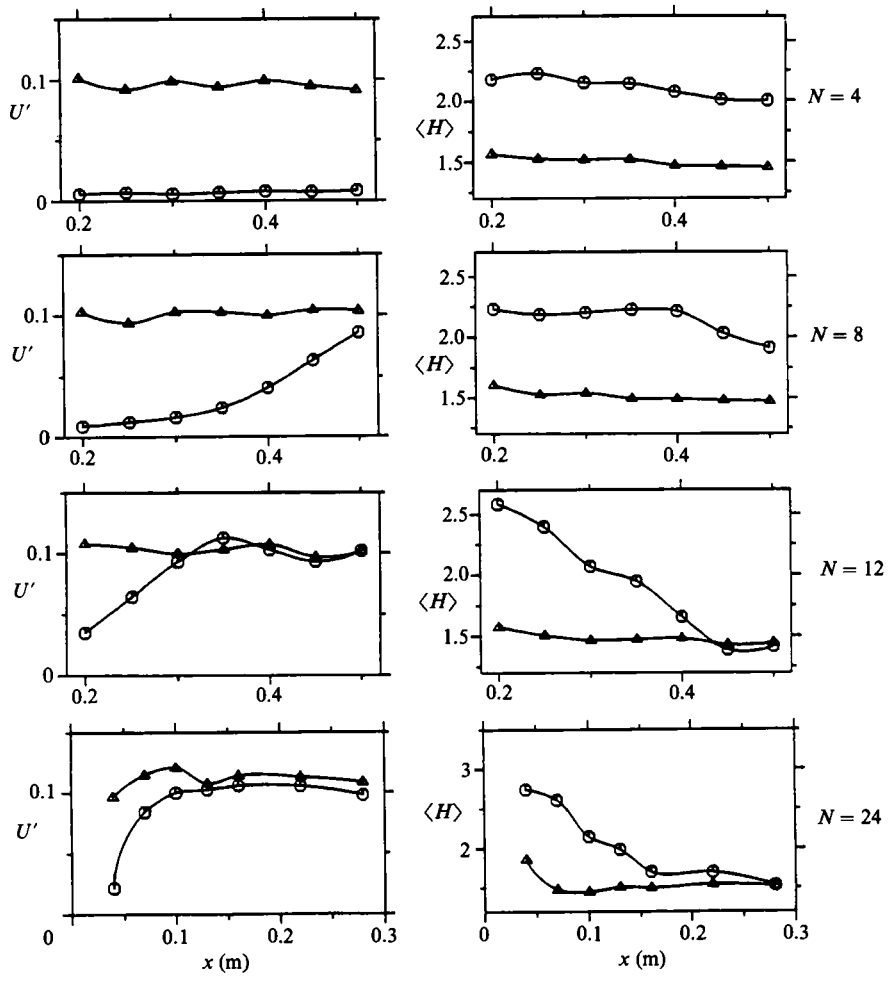

FIGURE 19. Variation of turbulence intensity U' and shape factor $\langle H \rangle$ in the Lagrangian frame for fluid parcels underneath the disturbed (△) and undisturbed (○) free-streams.

($\tilde{c}_p$) that no instantaneous destabilizing adverse pressure gradients can occur. It should also be noted that, apart from the region very close to the leading edge, the flow is closely parallel to the plate and $\tilde{v}$-velocities are very small (see e.g. the instantaneous velocity vectors given in Liu & Rodi 1989).

In the so-called laminar stripes underneath undisturbed free stream (circles), U' is initially much lower, and H is above 2 as in laminar boundary layers. For the case with $N = 4$ these quantities stay at these levels, i.e. these stripes remain laminar until the last measurement station. For the other cases, U' starts to increase after a certain distance and rises to the level of 0.1 in the turbulent patch. The location where this is more or less complete is included as a transition location in table 2. H decreases from the initial values above 2 towards a value of 1.5 typical for turbulent boundary layers, but these low values are reached later than where the near-wall fluctuations indicate completion of transition, which is consistent with the observations from figures 13 and 16.

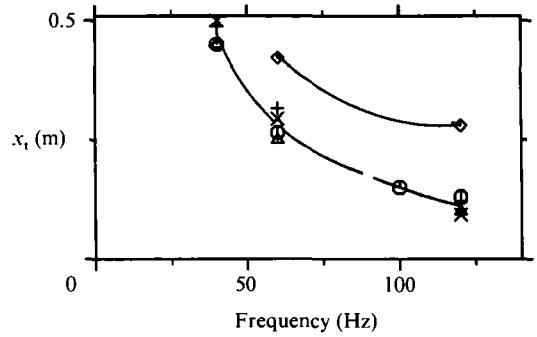

FIGURE 20. Variation of transition location x_t with frequency; symbols see table 2.

Frequency (Hz)	20	40	60	100	120	symbol in figure 20
(1) Hot-wire trace, figures 7–10	—	450	265	150	130	○
(2) $P_L = 0$, figure 17	—	450	250	—	100	△
(3) U' min = 0.09, figure 18	—	488	316	—	120	+
(4) $U_L^* = 0.09$, figure 19 (○)	—	500	294	—	93	×
(5) $H_L = 1.5$, figure 19 (○)	—	—	422	—	280	◇
(6) Average of (1), (2), (3) and (4)	—	472	281	150	111	———

TABLE 2. Transition positions x_t in mm

3.3.4. *Transition location*

From the results presented so far, a fairly clear and consistent picture has emerged about the transition process and the position where transition takes place in the fluid parcels underneath the undisturbed flow. Table 2 compiles the transition locations interpreted from various different graphs as discussed above, where transition is here meant to stand for the merger of the turbulent stripes and the locations where the turbulence intensity reaches the level prevailing in turbulent boundary layers. The transition locations are plotted in figure 20 versus the wake-passing frequency. An additional result from test case 6 has been added. Figure 20 yields a clear dependence of the transition location on the frequency of the passing wakes. At the higher frequencies, the curve levels off and it appears that were the frequency to be increased even further, the transition location would not shift much forward because the wakes have then already merged when they reach the plate so that the free stream does not carry discrete disturbances but simply free-stream turbulence.

The above discussion has shown that transition of the entire boundary layer including the adjustment of velocity profiles is complete only at some distance downstream of the transition location inferred from the near-wall fluctuations. Approximate locations taken from figure 19 where the shape factor H reaches a turbulent value of about 1.5 are also included in table 2 and in figure 20. As there may be an interest in the values of $Re_{\bar{\theta}}$ and $\bar{H}$ at the end of transition, these values are compiled in table 3 for both transition locations just discussed.

3.3.5. *Velocity profiles in wall coordinates*

For two selected local situations and for two times in each case, the profiles of the ensemble-averaged velocity are given in wall coordinates, i.e. $U^+ = \langle U \rangle / \langle U_\tau \rangle$ is plotted versus $y^+ = y\langle U_\tau \rangle / \nu$, where U_τ is the friction velocity. The friction velocity

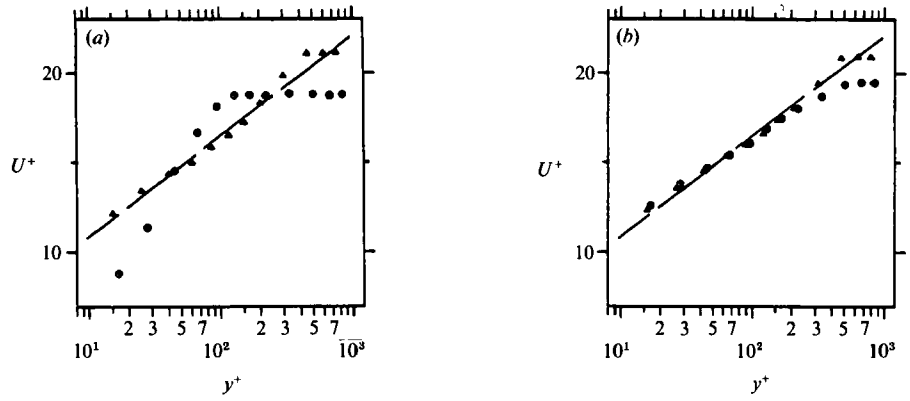

FIGURE 21. Selected velocity profiles in wall coordinates. (*a*) Case 2 ($N = 4$) at $x = 350$ mm: ○, $t/T = 0.25$ underneath undisturbed free stream; △, $t/T = 0.68$ underneath disturbed free stream. (*b*) Case 4 ($N = 12$) at $x = 500$ mm: ○, $t/T = 0.54$ underneath undisturbed free stream; △, $t/T = 0.90$ underneath disturbed free stream. ——, Standard logarithmic distribution.

Case no.		3	4	5
Frequency (Hz)		40	60	120
Location where turbulent stripes merge	x_t (mm)	450	265	130
	$Re_{\bar{\vartheta}}$	590	413	287
	$\bar{H}$	1.63	1.75	1.93
Location where $\bar{H} \approx 1.5$	x_t (mm)	500	400	280
	$Re_{\bar{\vartheta}}$	633	633	542
	$\bar{H}$	1.57	1.51	1.51

TABLE 3. Values of $Re_{\bar{\vartheta}}$ and $\bar{H}$ at the end of transition

was determined by Clauser's method from the measured velocity profiles. In figure 21 (*a*), the profiles are given for $N = 4$ at $x = 350$ mm where the boundary layer changes between a laminar and a turbulent state as discussed above. For a time t/T between the passing of two wakes (see figure 13) the boundary layer is laminar, and it can be clearly seen from figure 21 (*a*) that the velocity profile does not have a logarithmic distribution. On the other hand, at the time t/T the wake passes and the boundary layer is turbulent so that the velocity profile follows closely the standard logarithmic distribution ($\kappa = 0.41$, $C = 5.25$) also plotted in figure 21 (*a*).

For the second example, provided in figure 21 (*b*), the laminar patches have disappeared at the station considered ($x = 500$ mm) so that the boundary layer is always turbulent. Hence, for the two times shown in the figure, the velocity profiles follow closely the logarithmic distribution. Near the boundary-layer edge, the velocity profiles are of course somewhat different because of the variation in the free-stream velocity.

3.3.6. *Time-averaged integral parameters*

The time-averaged behaviour of the boundary layer can be judged best by looking at the downstream development of the time-averaged integral parameters. Figures 22 (*a–d*) show the development for the cases with $N = 4$, 8, 12, 24 respectively. For

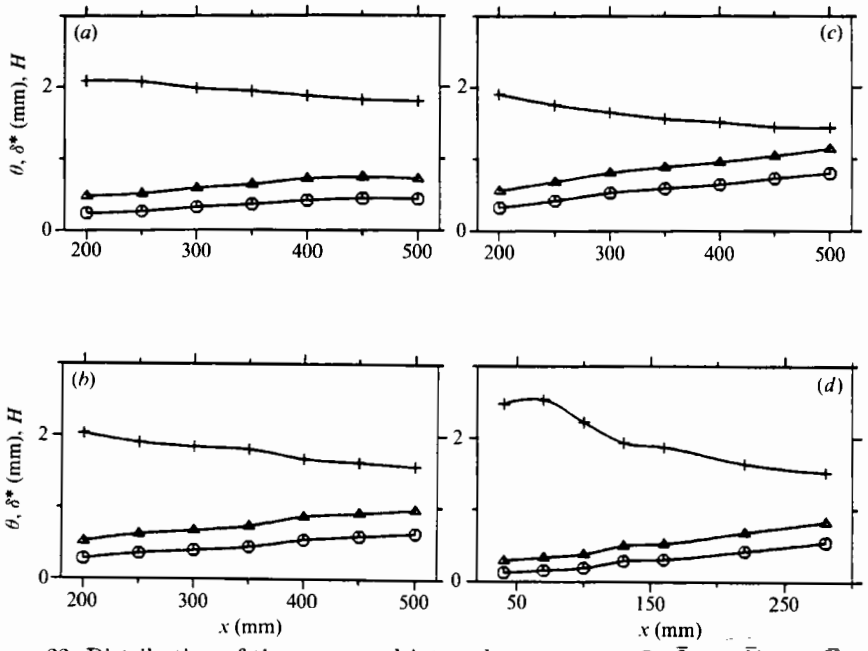

FIGURE 22. Distribution of time-averaged integral parameters: ○, $\bar{\theta}$; △, $\bar{\delta}^*$; +, $\bar{H}$. (*a*) Case 2 ($N = 4$), (*b*) case 3 ($N = 8$), (*c*) case 4 ($N = 12$), (*d*) case 5 ($N = 24$).

$N = 4$, the thicknesses $\bar{\delta}^*$ and $\bar{\theta}$ increase monotonically, and the shape factor $\bar{H}$ decreases monotonically from values slightly above 2 to values slightly below 2. This range indicates that the boundary layer is always intermittently laminar and turbulent, and the decrease in H indicates that the turbulent periods get longer further downstream. For $N = 8$, the thicknesses increase more strongly, and also now H decreases more, down to a level of about 1.6 which is already close to the value found in turbulent boundary layers. The behaviour is very similar for $N = 12$, where $\bar{H}$ now reaches a value of 1.5 at around $x = 450$ mm. In figure 22(*d*) for $N = 24$, relatively strong changes occur between $x = 100$ and 130, indicating that transition takes place in this region, in agreement with the previous findings. In this case, where the measurements started considerably earlier, the value of H is first clearly above 2 and then drops, first more rapidly then fairly gently to a value of about 1.5.

3.3.7. *Profiles of time-averaged periodic and turbulent fluctuations*

Figure 23 displays profiles of the time-averaged periodic fluctuations at various downstream distances. The discussion here complements that given on the behaviour for periodic velocity fluctuations in connection with figures 13–16. The time-averaged edge of the boundary layer is also indicated in figure 23. For $N = 4$ (figure 23*a*), the periodic fluctuations can be seen to be fairly constant outside the boundary layer. Inside the boundary layer, the periodic fluctuations increase strongly as the wall is approached. This is the region where in figure 11 the velocity during times of turbulent boundary is lower than the velocity during times of laminar boundary layer. Owing to the switching-over of this behaviour as illustrated in figure 11 and as discussed before, the level of periodic fluctuations then decreases to a local minimum at the switching-over point, but it increases again very near the wall where a reversal of the velocity takes place so that it is higher in turbulent boundary-layer patches than in laminar ones.

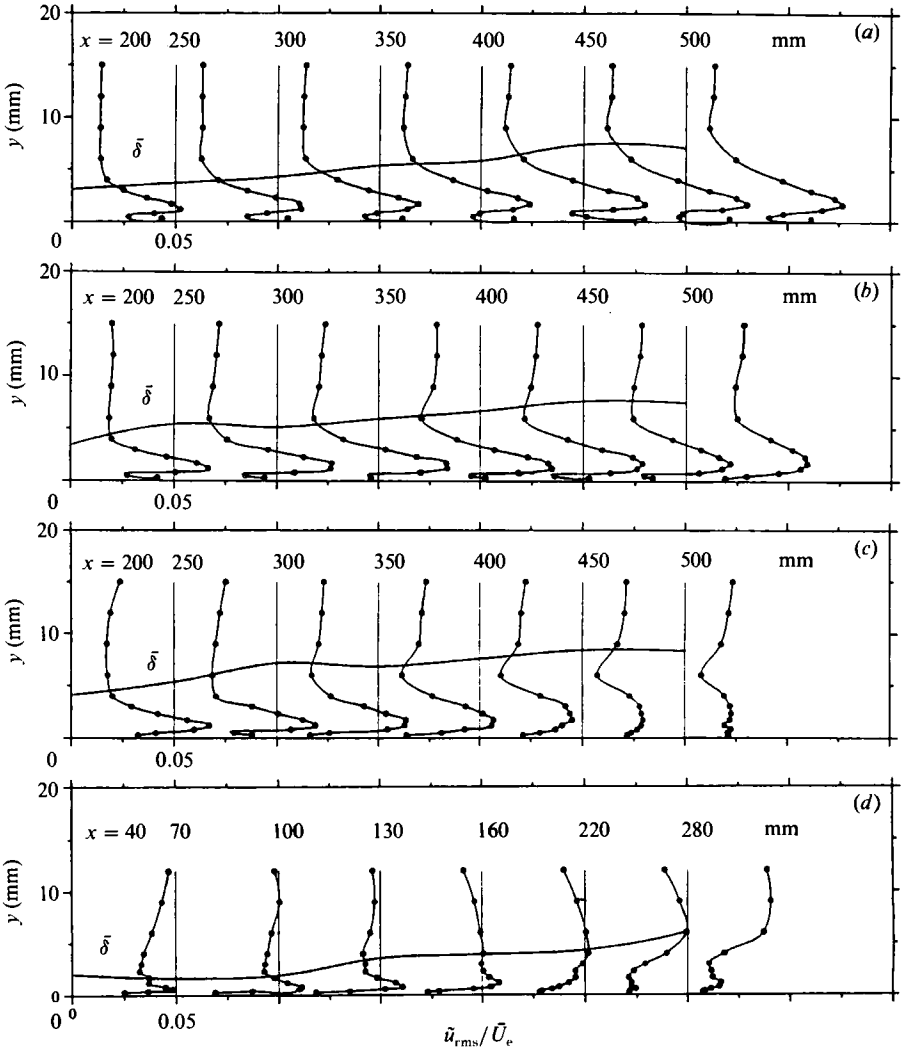

FIGURE 23. Profiles of r.m.s. values of periodic fluctuating velocity, $(\overline{\tilde{u}^2})^{\frac{1}{2}}/U_e$. (*a*) Case 2 ($N = 4$), (*b*) case 3 ($N = 8$), (*c*) case 4 ($N = 12$), (*d*) case 5 ($N = 24$).

For $N = 8$, the behaviour is similar, but now the level of periodic fluctuations decreases again beyond transition and the increase very near the wall does not occur there. Another noteworthy feature here is that the fluctuation level in the free stream is larger at the most downstream station than at the first station. This somewhat strange behaviour may be due to the influence of the secondary wake. For $N = 12$, in the region outside the boundary layer, the periodic-fluctuation level drops as the wall is approached, and a dip develops near the edge of the boundary layer. This behaviour is probably due to a combined interaction between the wakes themselves and between wakes and boundary layer. Inside the boundary layer, the periodic fluctuations increase again as discussed before, but also here the level decreases after transition has occurred in the initially laminar patches.

In the case of $N = 24$, the behaviour is more complicated. The periodic-fluctuation level is generally below the free-stream level, especially inside the boundary layer

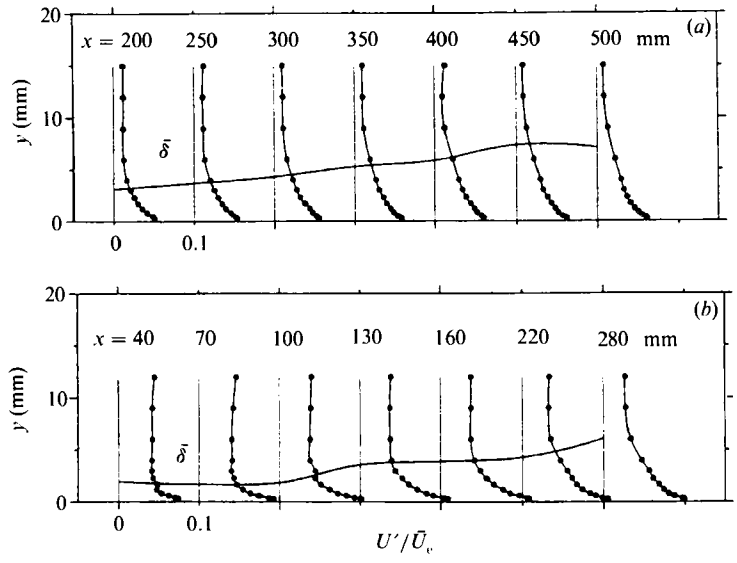

FIGURE 24. Profiles of r.m.s. values of turbulent fluctuations $\overline{\langle u'^2\rangle}^{\frac{1}{2}}/U_e$. (*a*) Case 2 ($N = 4$), (*b*) case 5 ($N = 24$).

beyond transition. However, at the further downstream locations there is a tendency for the periodic fluctuations to first increase towards the boundary-layer edge.

Figure 24 shows profiles of time-averaged turbulent fluctuations at various downstream locations. As these profiles depend much less on the number of cylinders, they are given only for $N = 4$ and $N = 24$. The profiles show how the turbulent fluctuations increase inside the boundary layer from their free-stream value determined by the wake turbulence to a considerably higher value near the wall. Also, this time-averaged near-wall value increases in the downstream direction as the periods of turbulent patches get longer. Once transition has occurred, these values are of course no longer changing. In these downstream regions beyond transition, the profile has the same behaviour as in developed turbulent boundary layers.

4. Conclusions

Detailed measurements were reported for boundary layers developing along a flat plate over which periodic wakes passed. These wakes were generated by cylinders moving on a squirrel cage in front of the leading edge. The Reynolds number was fairly low so that the boundary layer remained laminar over the full plate length when no disturbing wakes were present. With wakes passing over the plate, the free stream was intermittently disturbed by these wakes, with undisturbed periods in between. Underneath the wake-disturbed free stream, the boundary layer became turbulent quite early; in fact this transition happened before the first measurement station where the boundary layer was still so thin that it could not be resolved by the hot-wire measurements. The turbulent stripes underneath the wake-disturbed free stream travel downstream with the flow, the leading edge faster than the trailing edge so that the patches increase in width. The propagation velocities of the leading and trailing edges were found to be similar to those reported in the literature. Underneath the undisturbed free stream, the boundary layer remained laminar for some distance so that in an Eulerian frame the boundary layer is intermittently

laminar and turbulent. The laminar periods become shorter as the turbulent stripes grow together in the downstream direction. For the lowest wake-passing frequency, the turbulent stripes had not merged by the end of the test plate so that the intermittent boundary-layer behaviour continued to this point, but for the higher frequencies the turbulent stripes grew together and the laminar stripes disappeared at some location at which transition came to completion. It was found, however, that completion of transition in the outer parts of the boundary layer lagged behind the near-wall region. For higher wake-passing frequencies, the wake-generated patches merged faster so that transition occurred earlier, and a clear dependence of the transition location on the frequency was determined. The decrease of transition location x_{tr} with increasing frequencies levels off at the higher frequencies as the wakes then merge before they reach the plate and the free stream is disturbed in this case by free-stream turbulence at all times. In contrast to some other experiments (Pfeil *et al.* 1983; Addison & Hodson 1989*a*, *b*), natural transition (not triggered by the wakes) did not occur in the boundary-layer regions underneath the undisturbed free stream as the momentum thickness Reynolds number was rather low (see figure 4).

The transition behaviour can be followed quite nicely in a mean Lagrangian frame by travelling downstream with boundary-layer parcels underneath the disturbed and undisturbed free stream. In the first case, the boundary-layer state observed was more or less fully turbulent, while travelling with elements underneath the undisturbed free stream, the boundary layer was first laminar and then underwent transition (except for the lowest wake-passing frequency) as the turbulent stripes grew together. This approach lends itself to an easy modelling of the transition process and has already been used by Rodi *et al.* (1989) in their unsteady boundary-layer calculations.

The work reported here was sponsored by the German Federal Ministry of Research and Technology through program TURBOTHERM under contract no. 0326501D. The authors should like to thank Professor Pfeil and Mr Orth for helpful information on the squirrel cage design.

REFERENCES

Abu Ghannam, B. J. & Shaw, R. 1980 Natural transition of boundary layers – the effects of turbulence, pressure gradient, and flow history. *J. Mech. Engng Sci.* **22**, 213–228.

Addison, J. S. & Hodson, H. P. 1989*a* Unsteady transition in an axial flow turbine, Part 1 – Measurements on the turbine rotor. *ASME Paper* 89-GT-299.

Addison, J. S. & Hodson, H. P. 1989*b* Unsteady transition in an axial flow turbine, Part 2 – Cascade measurements and modelling. *ASME Paper* 89-GT-290.

Ashworth, D. A., LaGraff, J. E. & Schultz, D. L. 1989 Unsteady interaction effects on a transitional turbine blade boundary layer. *J. Turbomachinery* **111**, 162–168.

Brembati, F. 1975 An investigation of unsteady turbulent boundary layers. *Project Rep.* 1975-17. Von Kármán Institute of Fluid Dynamics, Rhode Saint Genese, Belgium.

Carr, W. 1981 A review of unsteady turbulent boundary layer experiments. In *Proc. IUTAM Symp. on Unsteady Turbulent Shear Flows* (ed. R. Michel), p. 3. Springer.

Cousteix, J. & Houdeville, R. 1988 Effects of unsteadiness on turbulent boundary layers. *VKI Lecture Series*, 1988-07.

Dong, Y. & Cumpsty, N. A. 1989*a* Compressor blade boundary layers: Part 1 – Test facility and measurements with no incident wakes. *ASME Paper* 89-GT-50.

Dong, Y. & Cumpsty, N. A. 1989*b* Compressor blade boundary layers: Part 2 – Measurements with incident wakes. *ASME Paper* 89-GT-51.

HERBST, R. 1980 Entwicklung von Grenzschichten bei instationärer Zuströmung. Ph.D. thesis, Technical University Darmstadt.

HODSON, H. P. 1983 The development of unsteady boundary layers on the rotor of an axial-flow turbine. *AGARD CP* 351.

KARLSSON, S. K. F. 1985 An unsteady turbulent boundary layer. Ph.D. thesis, Johns Hopkins University.

LAGRAFF, J. E., ASHWORTH, D. A. & SCHULTZ, D. L. 1988 Measurement and modelling of the gas turbine blade transition process as disturbed by wakes. *ASME Paper* 88-GT-232.

LIU, X. & RODI, W. 1989 Measurements of unsteady flow over and heat transfer from a flat plate. *ASME Paper* 89-GT-2.

PARIKH, P. G., REYNOLDS, W. C. & JAYARAMAN, R. 1981 On the behaviour of an unsteady turbulent boundary layer. In *Numerical and Physical Aspects of Aerodynamic Flows* (ed. T. Cebeci). University of California at Long Beach. Springer.

PFEIL, H. & SCHRÖDER, T. 1981 Decay of the wake behind a cylinder crossing rapidly the flow. *AIAA*-81-0209.

PFEIL, H., HERBST, R. & SCHRÖDER, T. 1983 Investigation of the laminar-turbulent transition of boundary layers disturbed by wakes. *Trans. ASME* A: *Engng for Power* **105**, 130–137.

RAJ, R. & LAKSHMINARAYANA, B. 1973 Characteristics of the wake behind a cascade of airfoils. *J. Fluid Mech.* **61**, 707–730.

RODI, W., LIU, X. & SCHÖNUNG, B. 1989 Transitional boundary layers with wake-induced unsteadiness. *Proc. Fourth Symp. on Numerical and Physical Aspects of Aerodynamic Flows, Long Beach, California, USA.*

SCHRÖDER, H. 1985 Entwicklung des instationären Nachlaufs hinter quer zur Strömungsrichtung bewegten Zylindern und dessen Einfluß auf das Umschlagverhalten von ebenen Grenzschichten stromabwärts angeordneter Versuchskörper. Ph.D. thesis, Technical University Darmstadt.

SCHUBAUER, G. B. & KLEBANOFF, P. S. 1955 Contributions on the mechanics of boundary layer transition. *NACA TN* 3489.

SPALART, P. R. & BALDWIN, B. S. 1989 Direct simulation of a turbulent oscillating boundary layer. In *Turbulent Shear Flows VI*, pp. 417–440. Springer.

WALKER, G. J. 1974 The unsteady nature of boundary layer transition on an axial-flow compressor blade. *ASME Paper* 74-GT-135.